J Sol-Gel Sci Technol (2015) 76:378–385
DOI 10.1007/s10971-015-3786-1

ORIGINAL PAPER

Optical properties of $Zn_{1-x}Al_xO$:NiO transparent metal oxide composite thin films prepared by sol–gel method

Bilal Arif[1] · H. M. El-Nasser[2] · A. Dere[1] · Ahmed A. Al-Ghamdi[3] · S. Bin-Omran[4] · Farid El-Tantawy[5] · F. Yakuphanoglu[1,3]

Received: 11 February 2015 / Accepted: 26 June 2015 / Published online: 17 July 2015

Abstract The films of $Zn_{1-x}Al_xO$:NiO (AZO; Al/Zn = 1.5 at.%, $x = 0.5$–2.0) were synthesized on glass substrates by sol–gel method. The morphological properties of the films were studied by atomic force microscopy. The surface morphology of the films is found to depend on the concentration of NiO. The optical band gap, Urbach energy and optical constants such as refractive index, extinction coefficient and real and imaginary parts of the dielectric constant of the films were determined. The refractive index dispersion of the films obeys the single-oscillator model, and the single-oscillator parameters were determined. The optical band gap of ZnO film was found to be 3.76 eV, and the optical band gap of the films increases with NiO doping. The obtained results suggest that $Zn_{1-x}Al_xO$:NiO films can be used as optical material in optical communication applications.

Graphical Abstract

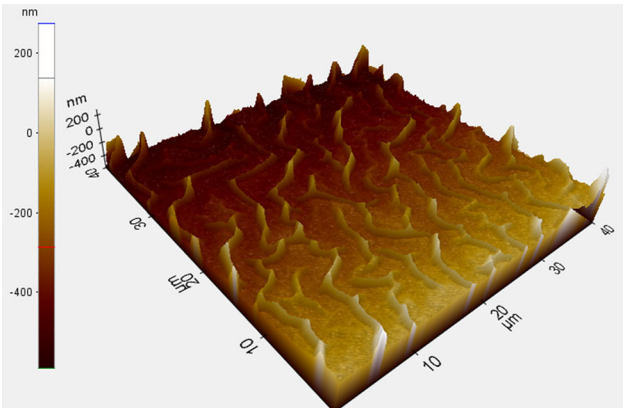

Keywords AZO film · Nickel oxide · Transparent metal oxide film

1 Introduction

Al-doped ZnO thin films (AZO) have been extensively studied for their potential use in optoelectronic devices. ZnO is a wide band gap semiconductor material, with direct band gap 3.37 eV at 300 K and large exciton binding energy 60 meV. The versatile properties of ZnO such as high electrical conductivity, high infrared reflectance, high visible transmittance, piezoelectricity, chemical stability, low resistivity, abundance in nature, easy fabrication and biocompatibility make it useful in the field of solar cells [1], gas sensors [2], photodetectors [3], light-emitting diodes [4], thin film transistor [5], piezoelectric devices [6], varistors [7] and surface acoustic-wave devices [8] etc.

✉ F. Yakuphanoglu
fyhan@hotmail.com; fyhanoglu@firat.edu.tr

1 Department of Physics, Faculty of Science, Fırat University, Elazig, Turkey

2 Department of Physics, Al al-Bayt University, Mafraq, Jordan

3 Department of Physics, Faculty of Science, King Abdulaziz University, Jeddah, Saudi Arabia

4 Physics and Astronomy Department, College of Science, King Saud University, Riyadh, Saudi Arabia

5 Department of Physics, Faculty of Science, Suez Canal University, Ismailia, Egypt

The defects in the crystal structure of the thin films play an important role in controlling the properties and the quality of ZnO films. Extrinsic doping with selective elements modifiying the electron energy band structure, affects the crystalline quality and native point defects and offers an effective way to tailor the electrical, optical and magnetic properties of ZnO. The undoped ZnO thin films are transparent and have usually low conductivity. Al doping in ZnO thin film can improve its conductivity without impairing the optical transmission, which is considered as the best candidate material for replacing indium tin oxide (ITO) [9–12]. The doping can reduce the crystalline quality of ZnO films and can change the defect environment, depending on whether Al atoms substitute for zinc atoms or occupy interstitial sites [13, 14].

Transparent conducting oxides (TCO) are of great interest for their use in electronic and electro-optical applications such as flat screens, thin film photovoltaic cells, dye-sensitized solar cells and light-emitting diodes (LEDs). However, the biggest challenge to achieve the ZnO-based optoelectronic devices is the difficulty to fabricate reliable p-type ZnO. In previous studies, many efforts focuses on doping ZnO with N [12], P [13], As [15] and Al-N [16] co-doped to achieve p-type conductivity. These dopants are used to alter the type of conductivity as well as the electrical and optical properties. Transition metals are promising candidate for doping ZnO. Cuprous oxide (Cu_2O) is a well-known p-type semiconductor among transition metal oxides, with band gap 2.17 eV and hole mobility 60 and 90 cm^2/V.s for polycrystalline and epitaxial films, respectively. In addition, its electrical properties can be controlled easily by modifying the valance states of Cu to Cu^+ and Cu^{2+} via a post-annealing treatment. p-type TCO thin film doped with Cu_2O has been reported fabricated using sol–gel method [17]. Among various transition metals, Ni is important dopant because isomorphic to Zn. Ni^{2+} (0.69 Å) has almost the same radius and valance compare to Zn^{2+} (0.74 Å), so can substitute the Zn^{2+} in the ZnO lattice. The efficiency of the dopant atoms depends on difference between their ionic radius and the ionic radius of host atoms (zinc or oxygen) [18]. Yakuphanoglu et al. [19] have reported photoluminescence and optical properties of nanostructure Ni-doped ZnO thin films prepared by sol–gel spin coating technique.

The potential use of nanostructures using confined transport phenomena to construct one-dimensional devices has gained much more interest. Recently, ZnO nanostructures such as nanorods, nanowires, nanoribbons, nanobelts and various interesting structures have been demonstrated. These ZnO-based nanostructures with different shapes provide higher surface area, exhibiting interesting physical and chemical properties which are unattainable by the other nanostructures. ZnO homojunction photodiodes based on Sb-doped p-type nanowire array and n-type film for ultraviolet detection have been reported [18, 20].

There are several methods of synthesis of ZnO nanostructures in the literature such as spray pyrolysis [21–23], sputtering [24–27], chemical vapor deposition [28, 29] and pulsed laser deposition [30]. But among all, the sol–gel method is simple and cost-effective and provides homogeneity and lower crystallization temperature. It is well known that the zinc oxide is n-type semiconductor. We have evaluated that the n-type conductivity of ZnO can be converted to p-type by NiO dopant. With this aim, Al-doped ZnO thin films (AZO) were doped with various NiO contents to alter the conductivity type of AZO films. Thus, in this paper, the structural and optical properties of NiO-doped AZO (NiO:AZO) films with different molar ratios of NiO synthesized via sol–gel method were studied.

2 Experimental procedure

The precursor sols were prepared from zinc acetate dehydrate ($Zn(CH_3COO)_2{\cdot}2H_2O$), 2-methoxyethanol and monoethanolamine (MEA). The concentration of Zn ion was 0.5 mol/L. Monoethanolamine was used as stabilizer. The molar ratio of MEA to zinc acetate was maintained at 1:1 to stabilize and produce a clear solution. In the solution prepared above, the required amount of aluminum nitrate non-hydrate ($Al(NO_3)_3{\cdot}9H_2O$) with Al/Zn atomic ratio of 1.5 % was added to obtain AZO solution. The resulting solution was stirred for 1 h at room temperature until a clear homogenous solution was formed. Then finally nickel(II) chloride hexahydrate ($NiCl_2{\cdot}6H_2O$) was dissolved into AZO solution at different molar ratios (0.5, 1.0, 1.5 and 2.0 %), and the solution was stirred overnight.

To synthesize the thin films, the glass slides were ultrasonically cleaned using methanol and acetone and with deionized water subsequently 5 min each and dried with nitrogen. The films were spin-coated at 1000 rpm for 5 s. After each layer was deposited, the substrate was heated at 160 °C as in Ref. [16]. The coating process was repeated three times. The films were finally annealed at 450 °C for 30 min to evaporate the solvent and remove the organic residue and then cooled in the furnace to room temperature. The optical properties were measured by UV-3600 Shimadzu spectrophotometer. The thickness of films was examined by park systems XE-100E atomic force microscope (AFM). The film thickness was measured by making a narrow scratch on the film surface. The film thickness of the films was measured as shown in Fig. 1 [31].

3 Results and discussion

For TCO optical transmittance is an important parameter. Optical transmittance spectra of the AZO doped with NiO annealed at 450 °C are shown in Fig. 2. All the films have

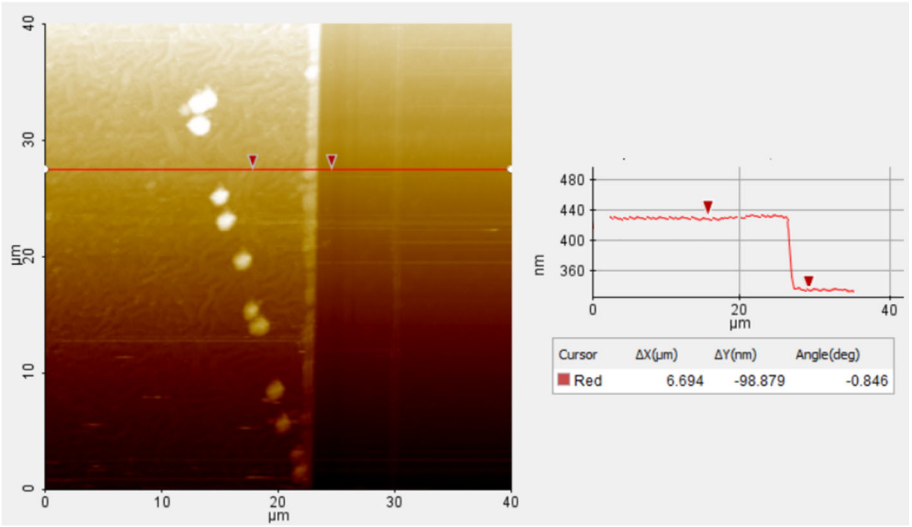

Fig. 1 Film thickness measurement **a** AFM image of AZO:NiO (0.5 %) film, **b** sample under AFM measurement

an average transmittance of 85 % in the visible range. The average transmittance of AZO film is smaller than that of aluminum-doped ZnO (AZO) thin films prepared using a pulsed DC unbalanced magnetron sputtering system [31]. It is evaluated that the transmittance of the studied films is resulted from the crystalline quality and structural properties of the films. Also, the transmittance of the films is affected by surface roughness, because the surface roughness causes a reduction in the scattering of light and in turn, the transmittance of the films is decreased due to fiber structure related to the crystallinity of the AZO film. The transmittance spectra also reveal that the transmittance does not change with various concentrations of doping. It is evident that doping with NiO does not affect the transmittance of the thin films, and hence we can effectively tune the electrical and optical properties of AZO thin films.

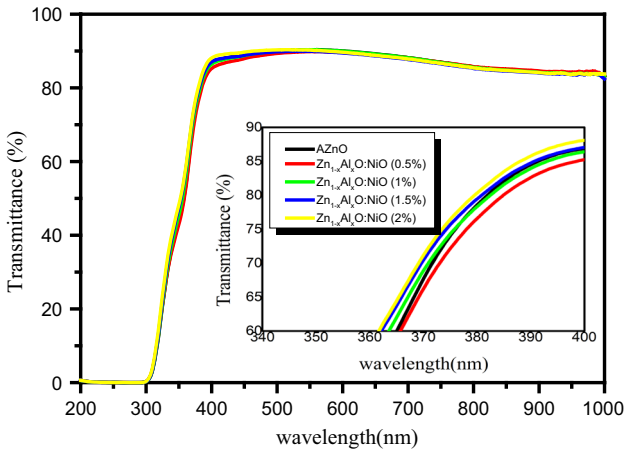

Fig. 2 Transmittance spectra for AZO and NiO-doped AZO films: The *inset* shows a magnification of absorption edge

Thus, highly transparent and conductive AZO-doped NiO thin films are potentially useful for transparent metal oxide films. The onset shows that absorption edge shifts toward the shorter wave length.

The relation between optical band gap and absorption coefficient is expressed by the following relation,

$$(\alpha h\upsilon) = D(h\upsilon - E_g)^{1/2} \quad (1)$$

where α is absorption coefficient, $h\upsilon$ is the photon energy, and D is a constant. The absorption coefficient α is given by the following relation [28].

$$\alpha = \frac{1}{d}\ln\left(\frac{(1-R^2)}{2T} + \sqrt{\frac{(1-R)^4}{4T^2} + R^2}\right) \quad (2)$$

The dependence of $(\alpha h\upsilon)^2$ on the photon energy ($h\upsilon$) for the AZO films with different concentrations of NiO is shown in Fig. 3. The band gap value of the films can be determined by extrapolating the graph of the linear region of the plots to energy axis at $(\alpha h\upsilon)^2 = 0$. The band gap values for AZO- and AZO:NiO (0.5, 1.0, 1.5 and 2.0 %)-doped films

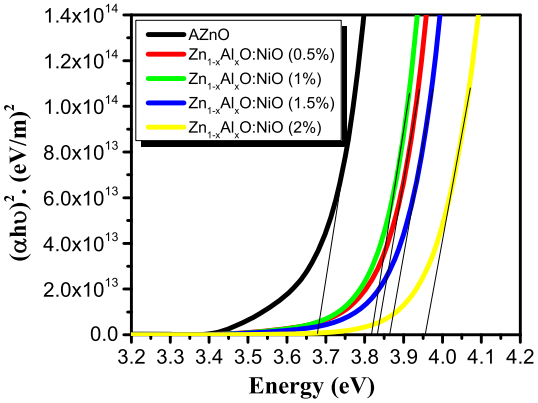

Fig. 3 Plots of $(\alpha h\upsilon)^2$ versus photon energy of AZO and NiO-doped AZO films

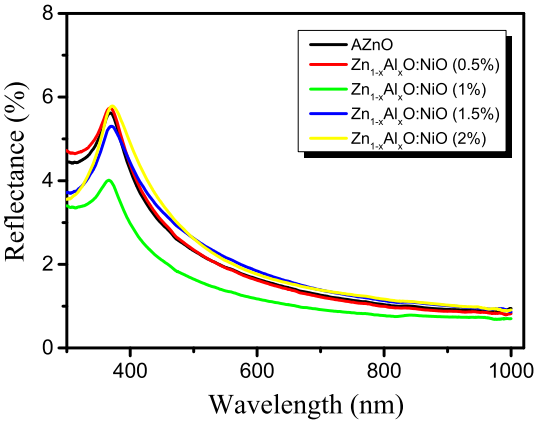

Fig. 4 Reflectance spectra for AZO and NiO-doped AZO films

Fig. 5 **a** Two-dimensional AFM images (40 μm × 40 μm) of 0 at.% (**a**), 0.5 at.% (**b**), 1 at.% (**c**), 1.5 at.% (**d**) and 2 at.% (**e**) NiO-doped AZO thin films. **b** Two-dimensional AFM images (40 μm × 40 μm) of 0 at.% (**a**), 0.5 at.% (**b**), 1 at.% (**c**), 1.5 at.% (**d**) and 2 at.% (**e**) NiO-doped AZO thin films

are 3.67, 3.82, 3.81, 3.86 and 3.95 eV, respectively. The increase in optical band gap of the AZO films with NiO content is explained by Burstein–Moss effect [29]. When the doping level is increased, the band tails the bottom of the conduction band and top of the valence band is narrowed with NiO content. Therefore, the optical band gap of AZO film is expanded, and that is why, the E_g value of is increased with NiO content.

The reflectance $R(\lambda)$ spectra for the AZO- and NiO-doped thin films are shown in Fig. 4. The peaks between 300–400 nm are especially important and are related to the absorption edge.

In order to understand the structure and surface morphology, the samples were examined by three-dimensional AFM. The AFM images of AZO- and AZO:NiO-doped films are shown in Fig. 5a, b in two (2D) and three (3D) dimensions. The film thicknesses of AZO:NiO (0, 0.5, 1.0, 1.5 and 2.0 %)-doped films were found to be 100 ± 0.1, 98 ± 0.3, 102 ± 0.2, 105 ± 0.1 and 108±0.2 nm, respectively.

The average surface roughness, R_q, values of AZO:NiO (0, 0.5, 1.0, 1.5 and 2.0 %)-doped films are determined to be 71, 78, 78, 39 and 53 nm for undoped and doped films, respectively. As seen in AFM images, the AZO films are formed from the fibers. The roughness, R_q, values of the films are quite high, and these high values are resulted from the spaces between the fibers. As seen in AFM images, the fibers are distributed on substrate surface with the spaces between fibers, and these spaces will significantly change the surface roughness of the films. The R_q value of the films is changed with the NiO content. The AZO:1 at.%NiO film exhibited the highest surface roughness, whereas AZO:2 at.%NiO film exhibited the lowest RMS value. This indicates that the surface roughness of the films is changed with NiO content, because the NiO content controls the thickness of the fibers. The fibers in the AZO:NiO film are closer than those of 1.0 at.%NiO film. The surface morphology of the fibers is due to the deformation and defects of crystalline lattice, because the Zn ions are replaced with Ni ions [1, 2]. The morphology showed that the fibers for the 1 % Ni doping were denser, but then became smaller than film having 2.0 at.%NiO. This is due to the distribution of the fibers on silicon substrate.

The crystal defects like vacancies, interstitial atoms and grain boundaries introduce the localized states in the band gap, affecting the optical band gap structures and optical transitions. The width of these localized states is called Urbach tail. The Urbach tail of the films is given by the following relation.

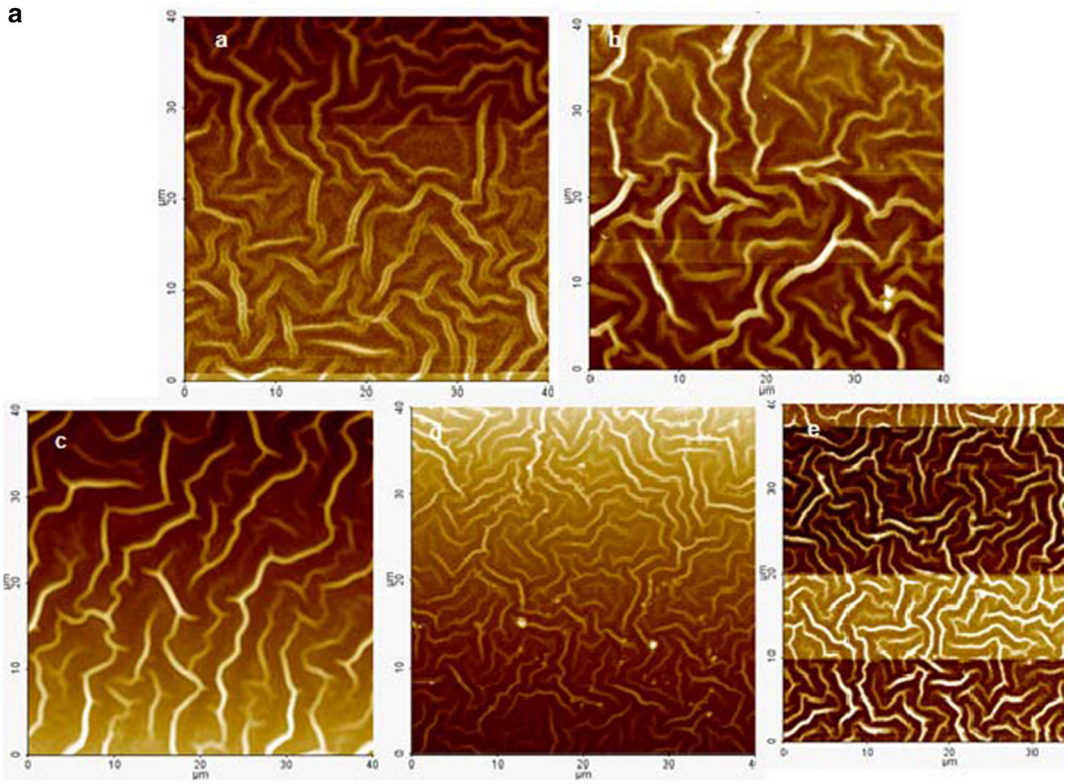
a
a
b
c
d
e

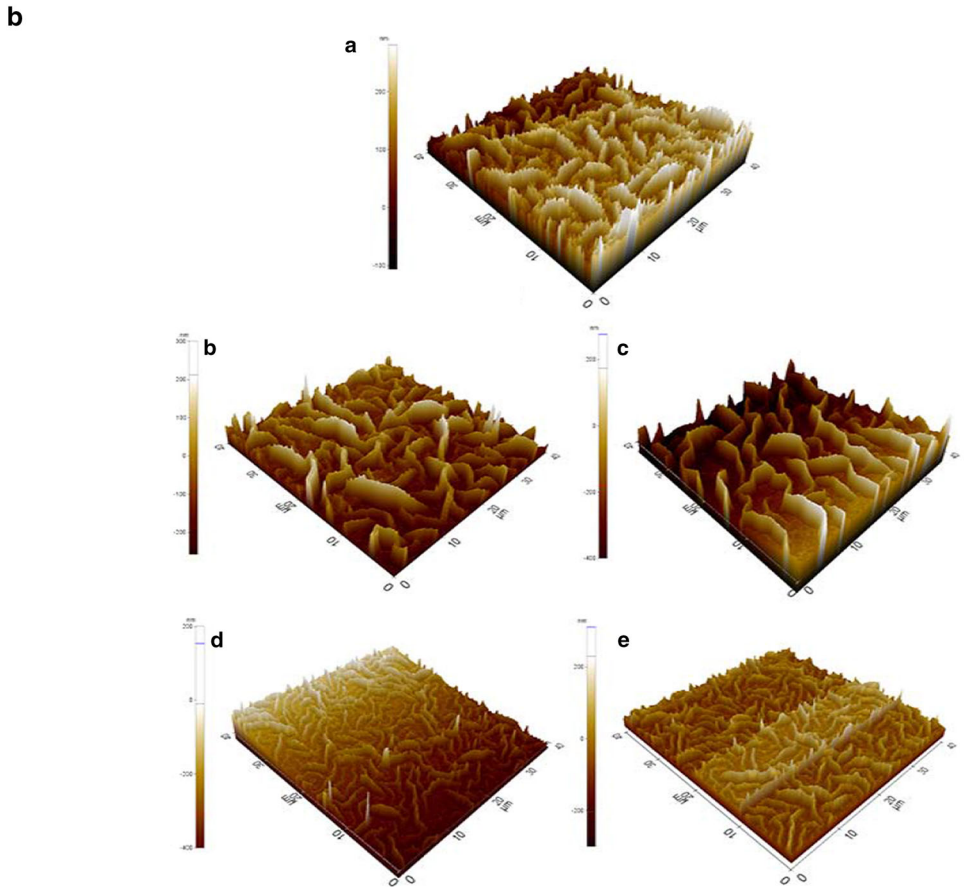
b
a
b
c
d
e

$$\alpha = \alpha_o \exp\left(\frac{E}{E_U}\right) \quad (3)$$

where E is the photon energy, α_o is the constant, and E_U is the Urbach energy refers to the width of exponential absorption edge. The above equation describes the transition between tails of occupied states in valance band to the unoccupied states at conduction band edge. The E_U values can be calculated by taking the inverse of the slop of the graph between lnα and $h\upsilon$ as shown in Fig. 6.

$$E_U = \left(\frac{d(\ln \alpha)}{d(h\upsilon)}\right)^{-1} \quad (4)$$

The E_U values of the films are decreasing with increase in doping concentration. The Urbach energy values change inversely to the band gap of films. The steepness parameter $\beta = kT/E_U$ ($T = 300$ K) was determined, which characterizes the broadening of the absorption edge due to the electron–phonon interaction or exciton–phonon interaction. The β value suggests that absorption edge changes with doping.

The study of dispersion is an important parameter for the application of any material in the field of integrated optical devices such as switches, filters and modulators used for optical communication. The refractive index of the film was determined by the following relation [28].

$$n = \left[\frac{1+R}{1-R}\right] + \sqrt{\frac{4R}{(1-R)^2} - k^2} \quad (5)$$

where $k = \alpha\lambda/4\pi$ is the extinction coefficient. The dependence of both refractive index and extinction coefficient on the wave length is plotted in Fig. 7. Both the refractive index and extinction coefficient decrease with increasing the wavelength. The refractive indices of all the films attain a peak around wavelength $\lambda = 365$ nm, lying in the absorption region, but at higher wavelength, value of n becomes constant, i.e., films behave as non-dispersive. In conclusion, the refractive index shows an anomalous behavior at lower frequency and normal dispersion at higher wavelengths.

The refractive index dispersion below the interband absorption edge corresponds to the electronic transition spectrum. This dispersion of refractive index has been analyzed using Wemple and Didomenico (WDD) single-oscillator model [30].

$$n^2 = 1 + \frac{E_o E_d}{E_o^2 - (h\upsilon)^2} \quad (6)$$

where E_o and E_d are the single-oscillator constants. The parameter E_o is an average band gap, the so-called WDD band gap, whereas E_d is oscillator strength and is related to interband optical transition. E_o and E_d are determined from the graph between $(n^2 - 1)^{-1}$ and $(h\upsilon)^2$ as shown in Fig. 8. The obtained values of E_o and E_d are given in Table 1. The oscillator energy E_o is an average energy gap and in a close

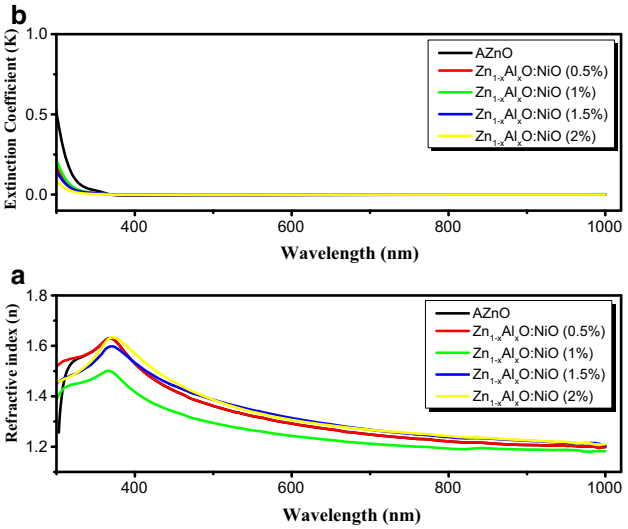

Fig. 7 Variation of refractive index (**a**) and extinction coefficient (**b**) with wavelength

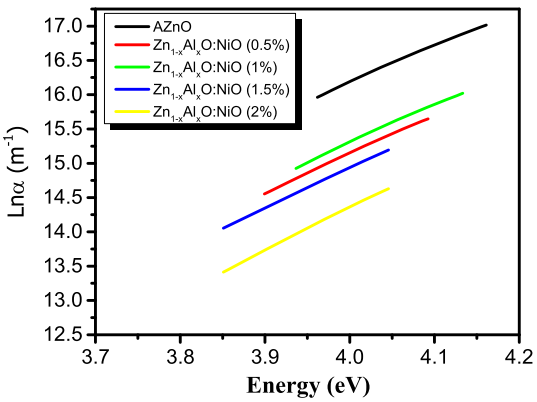

Fig. 6 Plots of lnα versus photon energy for AZO and NiO-doped AZO films

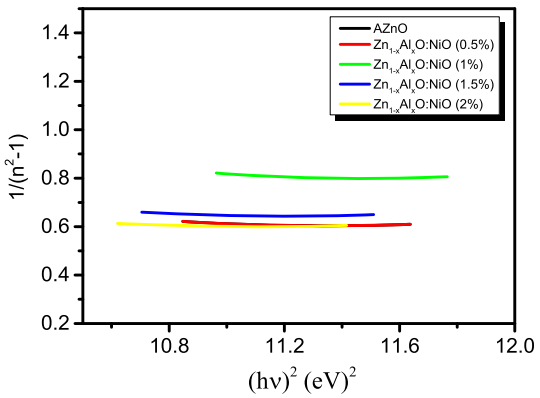

Fig. 8 Plots of $(n^2 - 1)^{-1}$ versus $(h\upsilon)^2$ for AZO and NiO-doped AZO films

Table 1 Optical parameters of the thin films

Sample	E_g (eV)	E_U (meV)	E_o (eV)	E_d (eV)	β
AZO	3.67	190	7.19	9.26	0.136
AZO:NiO 0.5 at.%	3.82	179	7.64	10.15	0.144
AZO:NiO 1 at.%	3.81	174	7.66	7.68	0.149
AZO:NiO 1.5 at.%	3.86	169	8.06	10.31	0.153
AZO:NiO 2 at.%	3.95	159	8.35	11.64	0.163

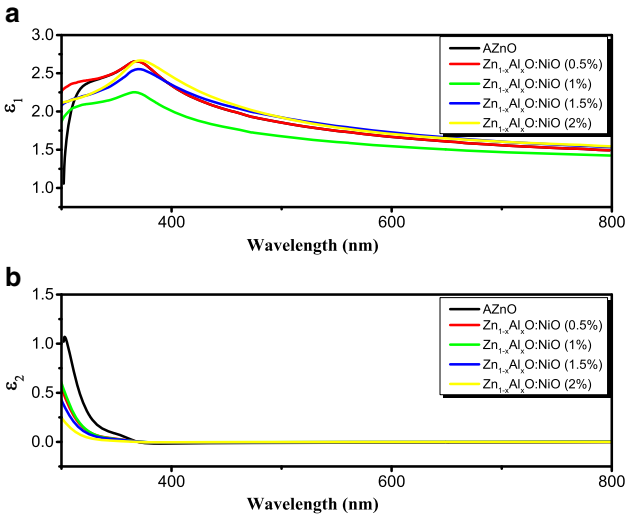

Fig. 9 Dielectric constant plots of the thin films **a** imaginary part, **b** real part

approximation with the optical band gap, in which $E_o \approx 1.5$, as suggested by WDD model.

The complex dielectric function is expressed as, $\varepsilon(\omega) = \varepsilon_1(\omega) + i\varepsilon_2(\omega)$, where ε_1 is the real part and ε_2 is the imaginary part of dielectric constant. The ε_1 and ε_2 values are determined by the following relations.

$$\varepsilon_1 = n^2 - k^2 \quad \text{and} \quad \varepsilon_2 = 2nk \tag{7}$$

The spectral dependence of ε_1 and ε_2 on the wavelength is shown in Fig. 9. The real part of dielectric constant is higher than the imaginary part. It is seen that real and imaginary parts of dielectric constant change with incident photon of at low wavelengths and cause formation of peaks in dielectric spectra, whereas dielectric constant values for both real and imaginary parts become constant at higher wavelengths. This variation of dielectric constant with the photon at lower wavelengths indicates that some interactions between photons and electrons in the films are produced in this wavelength range.

4 Conclusions

AZO- and NiO (0.5, 1.0, 1.5 and 2.0 %)-doped thin films were deposited by sol–gel technique. The surface morphology and optical properties of these films have been investigated. The AFM images show the fiber network effect in the surface. The doping does not lower the transmittance of films with average transmittance 85 % in the visible range. The blueshift in the optical band gap was attributed to Burstein–Moss effect and Urbach energy changed with doping. The optical constants of the films were determined. The refractive index values for all films show anomalous dispersion at lower wavelength and a normal dispersion at higher wavelengths. The refractive index dispersion obeys the single-oscillator model, and the single-oscillator parameters were determined.

Acknowledgments This study was supported by FIRAT University Scientific Research Projects Unit under Project No: FF.12.30. The authors gratefully acknowledge and thank the Deanship of Scientific Research, King Abdulaziz University (KAU), Jeddah, Saudi Arabia, for the research group "Advances in composites, Synthesis and applications." This work is as a result of international collaboration of the group with Professor F. Yakuphanoglu. This study was supported by King Saud University.

References

1. Wang W, Zhang G, Yu L, Bai X, Zhang Z, Zhao X (2007) Phys E 36:86–91
2. Shishiyanu ST, Shishiyanu TS, Lupan OI (2005) Sens Actuators B Chem 107:379
3. Rodriguez JA, Jirsak T, Dvorak J, Sambasivan S, Fischer DJ (2000) J Phys Chem B 104:319
4. Liu JP, Qu SC, Zeng XB, Xu Y, Gou XF, Wang ZJ, Zhou HY, Wang ZG (2007) Appl Surf Sci 253:7506
5. Banger KK, Yamashita Y, Mori K, Peterson RL, Leedham T, Rickard J, Sirringhaus H (2011) Nat Mater 10:45
6. Gardeniers JGE, Rittersma ZM, Burger GJ (1998) J Appl Phys 83:7844
7. Hung NT, Quang ND, Bernik S (2001) J Mater Res 16:2817
8. Shin W-C, Wu M-S (1994) J Cryst Growth 137:319
9. Wang T, Liu Y, Fang Q, Wu M, Sun X, Lu F (2011) Appl Surf Sci 257:2341–2345
10. Trolio AD, Bauer EM, Scavia G, Veroli C (2009) J Appl Phys 105:113109
11. Kim KH, Park KC, Ma DY (1997) J Appl Phys 81:7764–7772
12. Hwang DK, Kim HS, Lim JH, Oh JY, Yang JH, Park SJ, Kim KK, Look DC, Park YS (2005) Appl Phys Lett 86:151917
13. Kim KK, Kim HS, Hwang DK, Lim JH, Park SJ (2003) Appl Phys Lett 83:63
14. Jeong TS, Han MS, Youn CJ, Park YS (2004) J Appl Phys 96:175
15. Dutta M, Ghosh T, Basak D (2009) J Electron Mater 38:11
16. Hui KN, Hui KS, Li L, Cho YR, Singh J (2013) Mater Res Bull 48:96–100

17. Nunes P, Fortunato E, Tonello P, Fernandes FB, Vilarinho P, Martins R (2002) Vacuum 64:281–285
18. Farag AAM, Cavas M, Yakuphanoglu F, Amanullah FM (2011) J Alloys Compd 509:7900–7908
19. Wang G, Chu S, Zhan N, Lin Y, Chernyak L, Liu J (2011) Appl Phys Lett 98:041107
20. Vigil O, Cruz F, Morales-Acevedo A, Contreras-Puente G, Vaillant L, Santana G (2001) Mater Chem Phys 68:249
21. Bian JM, Li XM, Gao XD, Yu WD, Chen LD (2004) Appl Phys Lett 84:541
22. Pandey R, Yuldashev S, Nguyen HD, Jeon HC, Kang TW (2012) Curr Appl Phys 12:S56–S58
23. Bacaksiz E, Aksu S, Yılmaz S, Parlak M, Altunbaş M (2010) Thin Solid Films 518:4076–4080
24. Look DC, Renlund GM, Burgener RH, Sizelove JR (2004) Appl Phys Lett 85:5269
25. Kim D-K, Kim H-B (2015) Superlattices Microstruct 85:50–58
26. Tan ST, Sun XW, Yu ZG, Wu P, Lo GQ, Kwong DL (2007) Appl Phys Lett 91:72101
27. Gürbüz O, Güner S (2015) Ceram Int 41:3968–3974
28. Vaithianathan V, Lee BT, Kim SS (2005) J Appl Phys 98:043519
29. Najafi M, Haratizadeh H (2015) Solid State Sci 41:48–51
30. Devi V, Kumar M, Shukla DK, Choudhary RJ, Phase DM, Kumar R, Joshi BC (2015) Superlattices Microstruct 83:431–438
31. Lee J, Park YS (2015) Thin Solid Films 587:94–99